

Dynamics of iron atoms across the pressure-induced Invar transition in Pd₃FeM. L. Winterrose,¹ L. Mauger,¹ I. Halevy,¹ A. F. Yue,¹ M. S. Lucas,¹ J. A. Muñoz,¹ H. Tan,¹ Y. Xiao,² P. Chow,² W. Sturhahn,³ T. S. Toellner,³ E. E. Alp,³ and B. Fultz¹¹*W. M. Keck Laboratory, California Institute of Technology, Pasadena, California 91125, USA*²*HPCAT, Geophysical Laboratory, Carnegie Institution of Washington, Argonne, Illinois 60439, USA*³*Advanced Photon Source, Argonne National Laboratory, Argonne, Illinois 60439, USA*

(Received 17 August 2010; revised manuscript received 24 February 2011; published 20 April 2011)

The ⁵⁷Fe phonon partial density of states (PDOS) in *L*₁₂-ordered Pd₃Fe was studied at high pressures by nuclear resonant inelastic x-ray scattering (NRIXS) measurements and density functional theory (DFT) calculations. The NRIXS spectra showed that the stiffening of the ⁵⁷Fe PDOS with decreasing volume was slower from 12 to 24 GPa owing to the pressure-induced Invar transition in Pd₃Fe, with a change from a high-moment ferromagnetic (FM) state to a low-moment (LM) state observed by nuclear forward scattering. Force constants obtained from fitting to a Born–von Kármán model showed a relative softening of the first-nearest-neighbor (1NN) Fe–Pd longitudinal force constants at the magnetic transition. For the FM low-pressure state, the DFT calculations gave a PDOS and 1NN longitudinal force constants in good agreement with experiment, but discrepancies for the high-pressure LM state suggest the presence of short-range magnetic order.

DOI: [10.1103/PhysRevB.83.134304](https://doi.org/10.1103/PhysRevB.83.134304)

PACS number(s): 71.20.Be, 75.50.Bb, 62.50.–p, 76.80.+y

I. INTRODUCTION

The Fe–Pd alloy system exhibits interesting properties owing to a subtle interplay between magnetism and mechanical behavior. These properties, which are highly sensitive to chemical composition, include the shape-memory effect,¹ martensitic instability,² and vanishing thermal expansion (Invar effect).³ Interatomic forces are central to these phenomena, and studies of lattice dynamics can reveal some of the underlying reasons for the relationships between mechanical behavior and magnetism.

Stirling *et al.*⁴ measured phonon dispersions in ordered Pd₃Fe using inelastic neutron scattering. Fitting their results to a Born–von Kármán model, they found weaker nearest-neighbor Pd–Fe force constants compared to the nearest-neighbor Pd–Pd force constants. This difference was attributed to the size mismatch between Fe and Pd atoms and the distance dependence of the *d*-electron interaction. Yue *et al.*⁵ measured the ⁵⁷Fe phonon partial density of states (PDOS) in *L*₁₂-ordered Pd₃Fe and Pt₃Fe using nuclear resonant inelastic x-ray scattering (NRIXS) and reported effects from the mass difference of Pd and Pt atoms. The optical modes in Pd₃Fe involving Fe atoms were broadened in energy compared to those in Pt₃Fe. Ghosh⁶ performed a theoretical study of the lattice dynamics in ordered Pd₃Fe using density functional perturbation theory.⁷ The calculated phonon DOS and force constants were in reasonable agreement with the earlier experimental studies.

The control of pressure is a powerful means to alter both lattice dynamics and the magnetic state of materials. Pressure has long been used in studies of Invar materials,^{8–12} but recently, a new phenomenon was discovered at high pressures in Fe–Ni alloys away from the classical Invar composition.¹³ The application of pressure transformed the non-Invar alloys Fe_{0.55}Ni_{0.45} and Fe_{0.20}Ni_{0.80} into Invar alloys with zero thermal expansion. Several of the authors recently found this pressure-induced Invar phenomenon in Pd₃Fe, which is far removed from the narrow composition range of the Invar alloy Fe_{0.70}Pd_{0.30}.¹⁴ Under a pressure of 7 GPa

the alloy Pd₃Fe exhibits negligible thermal expansion from 300 K to approximately 523 K. The same study showed that the volume collapse at pressures from 10 to 15 GPa was accompanied by a magnetic transition from the ferromagnetic (FM) ground state to a low-spin (LS) state. Density functional theory (DFT) calculations showed how pressure pushed the majority-spin antibonding *t*_{2g} levels above the Fermi surface, accounting for the magnetic transition. The calculations did not give a reasonable prediction for the pressure of the magnetic transition, however, and this was attributed to an inadequate accounting for the spin structure in the high-pressure LS phase of Pd₃Fe.

Here we report results from an investigation on the lattice dynamics across the pressure-induced Invar transition in Pd₃Fe. The NRIXS method was used to measure the ⁵⁷Fe PDOS for samples in diamond-anvil cells at pressures up to 35 GPa. The DFT calculations of the PDOS were successful for the FM state at low pressure but were less successful for the low-spin state at high pressures. For the NRIXS spectra measured at high pressures, the highest energies of the Fe PDOS showed features consistent with the DFT predictions for FM material, suggesting there may be short-range magnetic order in the high-pressure phase of Pd₃Fe.

II. METHODS**A. Nuclear forward scattering**

Nuclear forward-scattering (NFS) measurements were performed at beamline 16ID-D at the Advanced Photon Source at the Argonne National Laboratory. The preparation of Pd₃⁵⁷Fe by the arc melting and homogenization of a small ingot was described previously.¹⁴ A Merrill-Bassett, Tel-Aviv-type diamond-anvil cell (DAC)¹⁵ was used to generate pressure on the sample. The sample was compressed in a sample chamber created by a Re gasket (~100-μm-diameter hole) and two opposing diamond culets of ~350-μm diameter. A 4:1 methanol-ethanol mixture was used as the pressure medium in the sample chamber. For low temperatures, the DAC was

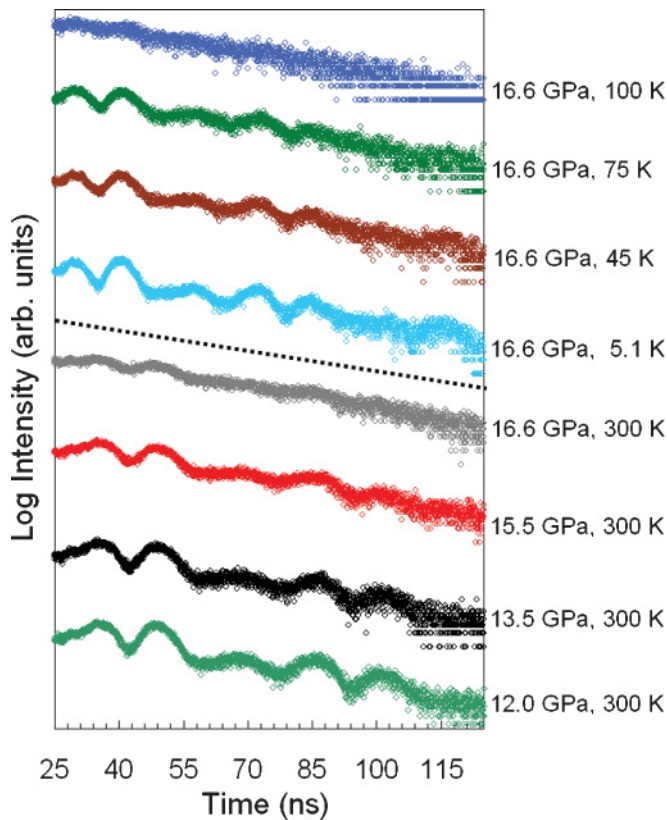


FIG. 1. (Color online) The ^{57}Fe nuclear forward scattering spectra from $L1_2$ -ordered $\text{Pd}_3^{57}\text{Fe}$. Quantum beats, indicative of the low-pressure magnetically ordered phase with moments stable longer than 1 ns, collapse above 15.5 GPa. Quantum beats reappear on lowering the temperature to 5.1 K and persist up to 75 K at 16.6 GPa.

cooled with a He-flow cryostat (Cryo Industries of America, Inc.). Two thermocouples measured temperatures throughout the low-temperature runs. An in-line Raman system was used for *in situ* pressure calibration at cryogenic temperatures by means of ruby fluorescence,¹⁶ and this method was also used for pressure determination in cells at ambient temperature.

As the pressure is increased at 300 K, the quantum beats diminish noticeably by 15.5 GPa and largely disappear at 16.6 GPa, indicating the collapse of magnetic order under pressure (Fig. 1). In the present measurements, the transition occurred at higher pressures than reported previously in Ref. 14, which showed diminished quantum beats at 12.3 GPa, and only weak beats were visible at pressures of 15.1 GPa or higher. The difference between the two sets of measurements is not caused by differences in the chemical compositions of the samples, which came from the same homogenized ingot. It could be caused by differences in internal stresses in the samples caused by the pressure media or by differences in the polycrystalline microstructures of the samples. Some down-pressure measurements showed evidence of hysteresis, where the intensity of the quantum beat pattern upon unloading was weaker than expected from comparison to data at similar pressures upon loading. The hysteresis and the pressure range of the transition are worthy of further study because they may give insight into the kinetics or nucleation properties of this phase transition, which was shown to be first-order in Ref. 14.

Figure 1 shows that, at a fixed pressure of 16.6 GPa, the quantum beats reappear upon reducing the temperature, although their periodicity is shorter, owing to a larger hyperfine magnetic field at cryogenic temperatures. As the temperature is increased at 16.6 GPa, the quantum beats fade, mostly disappearing by 100 K. The absence of quantum beats is also consistent with the presence of magnetic moments if they fluctuate faster than approximately 1 ns.

We also know that temperature suppresses the quantum beats at a temperature of 500 K as Pd_3Fe passes through its Curie transition,¹⁷ so we can give a rough picture of the P - T phase boundary for the Invar transition in Pd_3Fe . Around ambient temperature and below, the temperature dependence is weak, with the transition occurring at approximately 16.0 GPa at 300 K and approximately 16.6 GPa at 90 K. The temperature dependence must be stronger at higher temperatures, however, reaching 0 GPa at 500 K. These numbers should be considered as approximate, however. In one sample there was hysteresis in the magnetic transition, with the LS state persisting to low pressures after it formed at high pressure.

B. Nuclear resonant inelastic x-ray scattering

Using similar procedures as for the NFS samples, samples of $\text{Pd}_3^{57}\text{Fe}$ were prepared by arc melting Pd and ^{57}Fe of 95% isotopic enrichment. The sample was cold rolled into a thin foil of approximately 30- μm thickness and annealed in vacuum to induce $L1_2$ long-range order. X-ray diffraction measurements confirmed prominent superlattice diffraction peaks characteristic of the $L1_2$ structure.

Nuclear resonant inelastic x-ray scattering (NRIXS) spectra were measured at the 3-ID undulator beamline of the Advanced Photon Source at the Argonne National Laboratory. Final monochromization to a 1-meV bandwidth was performed with a high-resolution silicon (4 0 0)(10 6 4) monochromator.¹⁸ Samples were loaded into a piston-cylinder-type diamond-anvil cell¹⁹ for measurements to 35 GPa. The cell was sealed with Be gaskets that were 100 μm thick. Silicone oil was used as the pressure medium. Pressure was measured using the ruby fluorescence technique¹⁶ before and after the acquisition of spectra at each pressure. Spectra were collected by tuning the x-ray energy stepwise in the range of ± 80 meV around the ^{57}Fe Mössbauer nuclear resonance energy. Twelve scans were performed at each pressure, each scan approximately 1 h, and the successful scans were summed. Three avalanche photodiodes were used to count the delayed photons from nuclear deexcitation. The inelastic scattering intensity from $\text{Pd}_3^{57}\text{Fe}$ was converted into a ^{57}Fe phonon PDOS with the PHOENIX software package.²⁰ Results are presented in Fig. 2. The ambient ^{57}Fe PDOS matches well the NRIXS results from Ref. 5, displaying three peaks between approximately 15 and 30 meV, with the most intense peak occurring around 22 meV. With increasing pressure, the PDOS spectrum splits, and the high-energy peak shifts rapidly to higher energies.

C. Born-von Kármán fitting

The experimental ^{57}Fe phonon PDOS curves were fit to a Born-von Kármán model^{21,22} with first- and second-nearest-neighbor (1NN, 2NN) interactions. A set of interatomic force

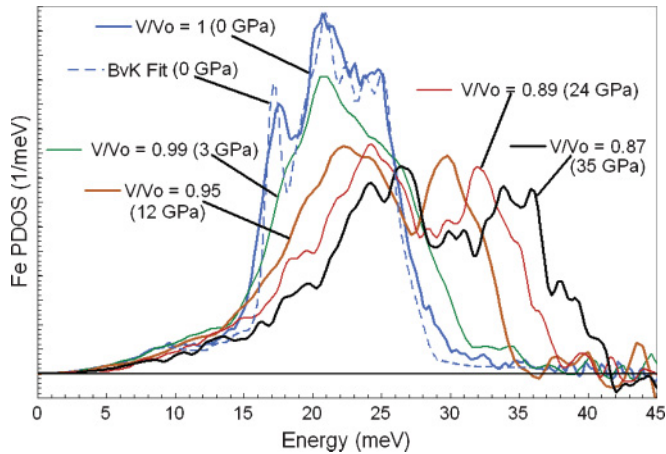


FIG. 2. (Color online) The ^{57}Fe phonon PDOS from NRIXS measurements on $L1_2$ -ordered Pd_3Fe . The Fe PDOS from a fit of the 0 GPa results to a Born-von Kármán (BvK) model is also shown.

constants was taken from DFT results and was used as the initial guess for the iterative procedure to obtain force constants. The calculated PDOS was convolved with the experimental instrument resolution function when comparing to the NRIXS spectra. The force constants were optimized to converge on the measured NRIXS PDOS result, using a differential evolution algorithm²³ implemented by the MYSTIC software package.²⁴

The Pd phonon PDOS is not measurable with NRIXS, so the Pd-Pd force constants are poorly constrained when fitting the Born-von Kármán model to ^{57}Fe phonon PDOS curves. The 1NN and 2NN Pd-Pd force constants were therefore fixed to the Pd-Pd force constants from DFT calculations. The resulting force constant matrices were decomposed into longitudinal and transverse components in two steps.²⁵ First, the force constant matrices were diagonalized, yielding three eigenvalues. Next, the force constant matrices were projected onto the bond directions. The eigenvalue matching the projection is the longitudinal force constant. The other two eigenvalues were averaged to give an averaged transverse force constant. This approach is reasonable so long as the forces are primarily axial,²⁵ as is typical of fcc metals. Table I shows that these DFT Pd-Pd force constants match reasonably well the dominant 1NN force constants from inelastic neutron scattering measurements⁴ at ambient pressure.

D. Density functional theory calculations

The VIENNA AB-INITIO SIMULATION PACKAGE (VASP)²⁶ was used for calculations on $L1_2$ -ordered Pd_3Fe with density functional theory in the local spin-density approximation (LSDA)²⁷ for the electronic exchange and correlation potential, using the projector augmented-wave (PAW) method.²⁸ In the calculations the semicore $3p$ states of Pd and $2p$ states of Fe were treated as valence. A unit cell was constructed and relaxed, followed by a series of single-point energy calculations around the equilibrium volume. The calculated results were fit to a Murnaghan equation of state,²⁹ and

TABLE I. Force constants projected along bond directions (longitudinal) and average perpendicular (transverse) force constants at $V/V_0 = 1.0$. BvK refers to results obtained by fitting our NRIXS curves to a Born-von Kármán model. The 2NN Fe-Fe force constants were not reported in Ref. 4.

Force constant	Longitudinal (N/m)	Transverse (N/m)
1NN Pd-Pd (Ref. 4)	57.28	-5.45
1NN Pd-Pd (DFT)	59.52	-5.00
2NN Pd-Pd (Ref. 4)	5.21	1.95
2NN Pd-Pd (DFT)	3.46	-0.01
1NN Fe-Pd (Ref. 4)	23.59	-0.40
1NN Fe-Pd (DFT)	17.73	-1.59
1NN Fe-Pd (BvK)	20.94	0.74
2NN Fe-Fe (DFT)	4.03	-1.72
2NN Fe-Fe (BvK)	9.56	-2.14

the ground-state volume, bulk modulus, and the pressure derivative of the bulk modulus were obtained, as described previously.¹⁴ This procedure gave a ferromagnetic ground-state lattice parameter a_0 of 3.802 Å and a smaller low-spin lattice parameter a of 3.760 Å. The calculations predicted a destabilization of the ferromagnetic state at $a = 3.690$ Å ($V/V_0 = 0.91$) in favor of an antiferromagnetic (AFM) state. The magnetic moments in the AFM state were predicted to decrease gradually with volume, vanishing entirely by $a = 3.148$ Å.

To study the vibrational properties of $L1_2$ -ordered Pd_3Fe , a series of 32-atom supercells were constructed. In the supercells, each symmetry-inequivalent atom was displaced from its equilibrium position in each symmetry-inequivalent direction. The Hellmann-Feynman forces induced on all other atoms were determined from a total-energy calculation. An energy cutoff of 330 eV was used for the plane-wave basis set, together with a $6 \times 6 \times 6$ Monkhorst-Pack grid. The first-order Methfessel-Paxton method with a smearing width of 0.1 eV was used for k -space summations. Energies were converged to better than 2 meV/atom with respect to both plane-wave cutoff and k -point grid. The resultant Hellmann-Feynman forces were used to generate the dynamical matrix using the direct method³⁰ as implemented in the PHONON software package.³¹ The dynamics model employed forces extending to fifth-nearest neighbors. The diagonalization of the dynamical matrix at a series of points in reciprocal space gave the phonon dispersion curves and the phonon DOS. Supercells for FM, AFM, LS, and nonmagnetic (NM) states were constructed. In the AFM state, the Fe moments were ordered in alternating ferromagnetic sheets in the (110) plane. Moments at the Fe and Pd sites were coupled ferromagnetically in the LS state with the combined magnetic moment in the unit cell never exceeding $0.1 \mu_B$. For calculations on materials under pressure, volume was constrained in the supercell calculations to better reveal the effect of the magnetic state on vibrational properties. To account for instrument resolution broadening and to allow for direct comparison with experimental results, the calculated vibrational spectra were broadened by a convolution with a Gaussian function with a standard deviation of 1 meV.

III. RESULTS AND DISCUSSION

A. Average phonon energies

The first moment, $\langle E \rangle$, of the Fe PDOS is shown in Fig. 3 as a function of decreasing volume (with respect to the volume at a pressure of 0 GPa, V_0). The DFT results fall on two curves, a high-moment curve with stiffer Fe PDOS for the ferromagnetic and antiferromagnetic states and a low-moment curve with softer Fe PDOS for the LS and NM states. In Fig. 3(a) the high-moment DFT solutions reproduce the NRIXS results well up to $V/V_0 = 0.95$ (12 GPa). Beyond $V/V_0 = 0.95$ the low-moment DFT solutions are more successful. The NRIXS $\langle E \rangle$ curve makes a transition between the high-moment and low-moment DFT curves, and this occurs at the pressures of the magnetic transition from the high-moment to the low-moment state found in the nuclear forward scattering measurements shown in Fig. 1. The slow stiffening of the ^{57}Fe PDOS from $V/V_0 = 0.95$ (12 GPa) to $V/V_0 = 0.89$ (24 GPa) accompanies the magnetic transition under pressure in Pd_3Fe . In Fig. 3 we see that the FM and AFM states have similar average

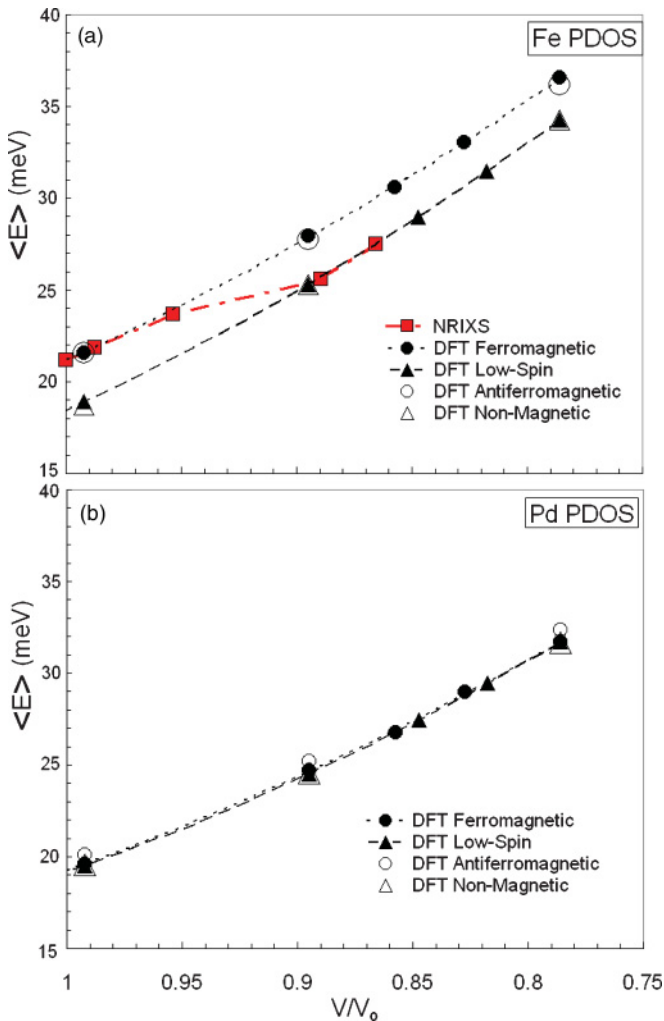


FIG. 3. (Color online) Measured and calculated average vibrational frequencies as functions of reduced volume for (a) Fe and (b) Pd phonon PDOS. The dashed lines are guides to the eye.

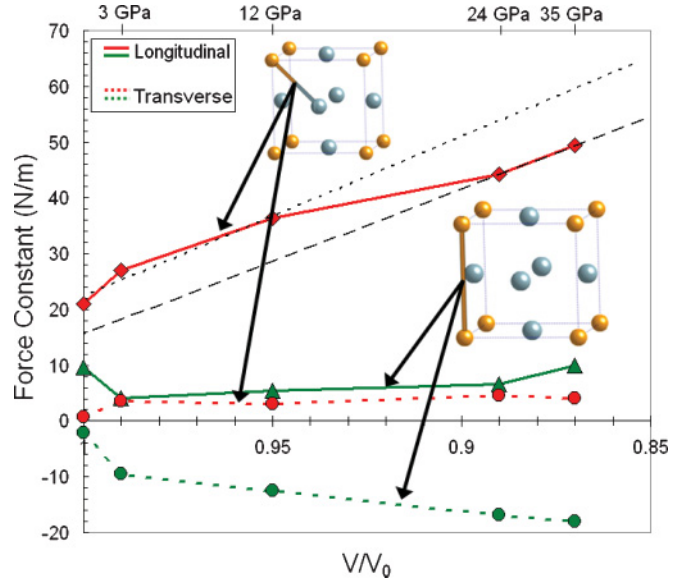


FIG. 4. (Color online) Fe force constants as a function of reduced volume calculated from fits of the NRIXS results to a Born-von Kármán model.

vibrational properties of Fe atoms. This is also true for the LS and NM calculations.

B. Force constants

The Fe-Pd and Fe-Fe force constants for 1NN and 2NN obtained by fitting the NRIXS curves to a Born-von Kármán model are presented in Fig. 4. Our 1NN Fe-Pd longitudinal force constants at ambient pressure (20.9 N/m) are in reasonable agreement with Stirling’s results (23.6 N/m).⁴ The large 1NN Fe-Pd longitudinal force constants stiffen significantly with pressure but show a change in slope between 12 and 24 GPa. This pattern follows the trend of $\langle E \rangle$ of the NRIXS Fe PDOS shown in Fig. 3(a). The smaller 0-GPa 1NN Fe-Pd transverse force constants (0.74 N/m) have opposite sign and are somewhat larger than Stirling’s (−0.4 N/m).⁴ The Fe-Fe 2NN longitudinal force constants are much smaller than the Fe-Pd 1NN longitudinal force constants. The Fe-Fe 2NN transverse force constants are large and negative.

The longitudinal force constants calculated by DFT methods for the FM and LS states were in reasonable agreement with the results of Fig. 4 for Born-von Kármán fitting to the NRIXS spectra, with the 2NN longitudinal force constant being much smaller. In contrast to the DFT Fe-Pd result, DFT results for the Pd-Pd 1NN longitudinal force constants showed stiffening in the low-spin state, as did the bulk modulus, which changed from 216 GPa in the FM and AFM states to 242.59 GPa in the LS state (as reported in Ref. 14). Unfortunately, the methods provide different transverse force constants, although these are smaller.

C. Electronic structure

Figure 5 shows DFT results for the electronic DOS at the Fe site for $L1_2$ Pd_3Fe , decomposed into states of t_{2g} and e_g

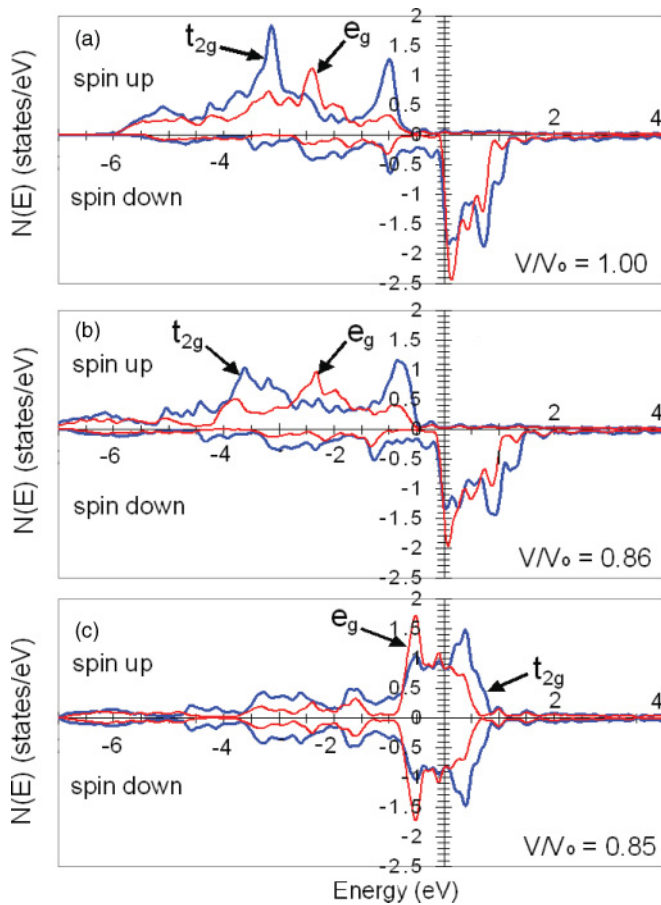


FIG. 5. (Color online) Electronic density of states at the Fe site decomposed into t_{2g} and e_g symmetry at various cell compressions. $E_F = 0$ eV.

character. (The Pd site is less interesting for the magnetic transition since it has a small moment in the ferromagnetic state.) The ferromagnetic state was stable at larger volumes, such as $V/V_0 = 1.0$ (i.e., the relaxed structure at 0 GPa). At $V/V_0 = 0.85$ the calculation was performed in the low-moment state with vanishing magnetic moments at the Fe and Pd sites.

These features of the electronic structure are similar to those proposed by Kaspar *et al.*³² and Entel *et al.*³³ for classical Invar alloys. For fcc transition metal alloys, the t_{2g} orbitals form strong dd bonds between 1NN atoms, owing to their large charge density in the [110] direction. This causes the t_{2g} electronic DOS to split into a high-energy subband with antibonding character and a low-energy subband with primarily bonding character. Both are occupied by majority spin electrons in the ferromagnetic state. (States with e_g character primarily have charge density between the more distant 2NN atoms along the [100] direction. They are less affected by pressure.) With decreasing lattice parameter, there is an increased splitting of the bonding and antibonding t_{2g} states. The occupied majority-spin antibonding t_{2g} states move closer to the Fermi energy, as shown in Fig. 5, and the pressure-induced Invar transition occurs as they become energetically unfavorable and their electrons are transferred into minority-spin states.

D. Lattice dynamics across the Invar transition

Figure 6(a) shows ferromagnetic Fe PDOS curves measured by NRIXS and calculated by DFT for $V/V_0 = 0.99$, with V_0 being the ferromagnetic ground-state volume. The NRIXS result is broader, but agreement between experiment and theory is good for this magnetic state. Figure 6(b) compares the measured Fe PDOS to the calculated FM and LS curves at $V/V_0 = 0.89$. The NFS data of Fig. 1 show that Pd_3Fe is in a nonmagnetic state at a compression of $V/V_0 = 0.89$, so it might seem best to compare the experimental curve to the LS DFT curve. Although the low-energy part of the measured Fe PDOS matches the LS result better than the FM result, in the LS curve the high-energy peak is too low in intensity and energy. Figure 6(b) shows that turning on ferromagnetism in the DFT calculation causes a stiffening and significant increase in the relative intensity of the calculated high-energy peak in the Fe PDOS. The average of the FM and LS PDOS calculations matches better the Fe PDOS at high energies.

The electronic states of t_{2g} character involve dd electron bonding along 1NN directions. The 1NN forces are dominant, so the changes in t_{2g} states across the Invar transition may dominate the changes in the dynamics of Fe atoms. With the collapse of the FM order comes a significant increase in the number of electronic states projected onto Fe atoms at the Fermi level, including more states with t_{2g} character. More states at the Fermi level allows more efficient screening of the

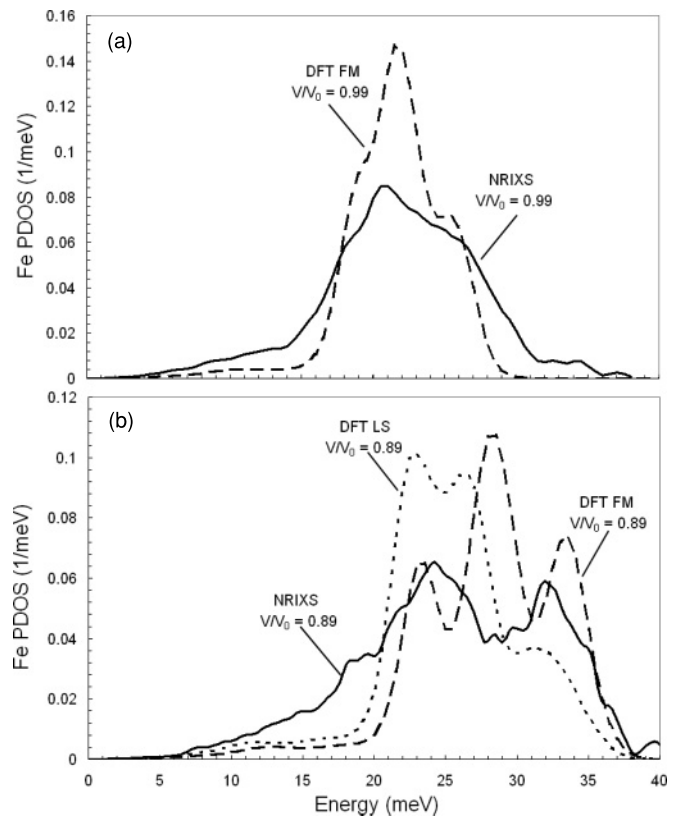


FIG. 6. Fe PDOS from NRIXS measurements and first-principles calculations. V_0 for the NRIXS curves refers to the ground-state volume determined by x-ray diffraction in Ref. 14. V_0 for the DFT curves refers to the ferromagnetic ground-state volume as determined by LSDA calculations.¹⁴

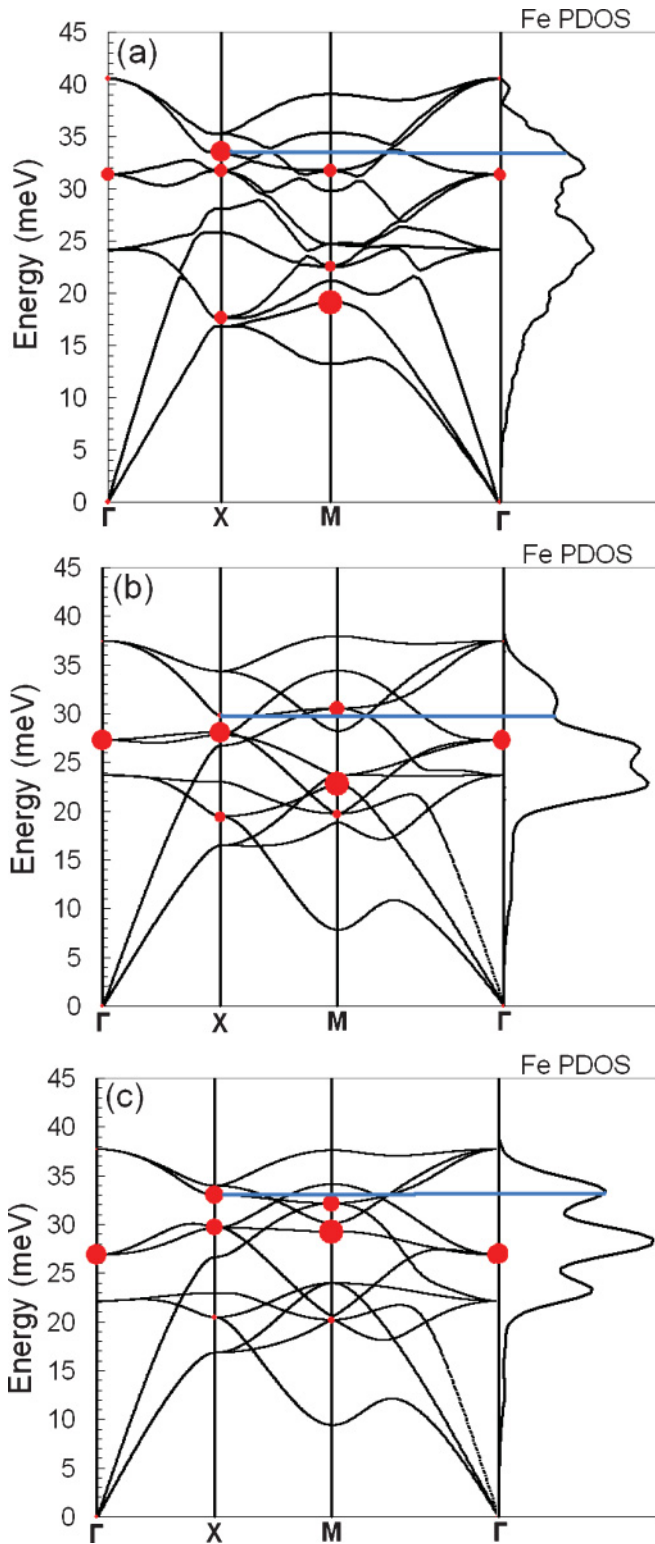


FIG. 7. (Color online) Dispersion curves and Fe phonon PDOS for the (a) NRIXS measured, (b) LS calculated, and (c) FM DFT calculated states. See text for explanation.

Fe atom displacements in phonons, softening them. This is seen as a major change in the Fe PDOS for the calculated FM to LS transition (Fig. 6), but this change is too large compared to experiment. Again, we suggest that short-range magnetic

order in the LS state may allow for stiffer 1NN force constants between Fe and Pd.

Figure 7 shows phonon dispersion curves along high-symmetry directions, generated by the force constants obtained from Born–von Kármán model fits to the NRIXS spectra [Fig. 7(a)] and by DFT methods for the LS and FM states [Figs. 7(b) and 7(c)]. To the right of the dispersions are shown Fe PDOS curves, obtained as the sum of the mean-squared vibrational amplitudes of Fe atoms in all modes. The magnitudes of the red dots in Fig. 7 are proportional to the square of the vibrational amplitudes of the Fe atoms in selected modes. Figure 7 shows that the most important contribution to the high-frequency peak in the Fe PDOS originates from the high-energy modes around the Brillouin zone boundary (X and M points).

The phonon modes between 30 and 35 meV around the X point in Fig. 7(a) contribute substantially to the high-frequency peak in the Fe PDOS. Figure 8 depicts the Fe atomic displacements associated with the mode at 33.2 meV at the X point in Fig. 7(a), and this mode is marked with horizontal blue lines in Fig. 7. This mode involves planes of Fe atoms moving directly against one another within the unit cell. This mode and its neighbors dominate the high-frequency peak in the Fe PDOS in the NRIXS results at $V/V_0 = 0.89$ [Fig. 7(a)]. The DFT LS curve [Fig. 7(b)] predicts it to be too small, whereas calculations for the FM state show a peak at 34 meV that is somewhat stronger than measured [Fig. 7(c)]. This difference can be traced to a stiffening of this mode in the FM state and also to a 70% decrease in the squared vibrational amplitude of the Fe atom motions in the LS state.

This comparison of DFT and NRIXS results suggests that short-range magnetic order persists in Pd₃Fe beyond the pressure-induced collapse of long-range ferromagnetic order. The phonon modes involving localized Fe atom movements, such as shown in Fig. 8, may be sensitive to short-range ferromagnetic order that exists in the LS state since the contribution of these modes to the Fe PDOS lies between the LS and FM DFT predictions. It is also important to consider the differences in time scales of the vibrations and the measurable magnetic fluctuations. The characteristic measurement time for the NFS measurements is at least 10^{-9} s, which is much longer than the vibrational periods of the higher-energy phonons measured by NRIXS (10^{-13} s). High-frequency phonons may see local magnetic order, even though it is averaged out for the slower NFS measurements. On

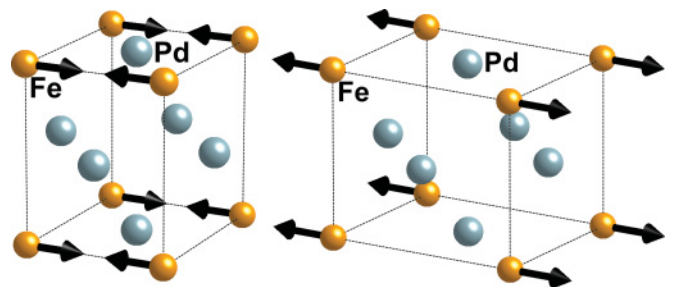


FIG. 8. (Color online) Two snapshots of the atomic displacements in a Pd₃Fe unit cell associated with the high-frequency mode at the X point of the Brillouin zone (see text). Arrows indicate the motion of the Fe atoms.

the other hand, the long-wavelength modes are better modeled by the LS DFT predictions.

IV. CONCLUSIONS

The ^{57}Fe phonon partial density of states (PDOS) in $L1_2$ -ordered Pd_3Fe was studied at high pressures using nuclear resonant inelastic x-ray scattering (NRIXS) measurements and density functional theory (DFT) calculations. On average, the Fe PDOS stiffens with pressure more slowly between 12 and 24 GPa, owing to the pressure-induced Invar transition in Pd_3Fe . Both the fits to experimental spectra and the DFT calculations show that Fe-Pd INN longitudinal force constants are stiffened by ferromagnetism, although the opposite trend occurs for the bulk modulus and the dominant Pd-Pd INN force constants. The change in Fe atom dynamics across the magnetic transition can be understood to originate with the same changes in the electronic states of t_{2g} character near the Fermi level that are important for the pressure-induced Invar transition itself. Although the DFT calculations work well for predicting the Fe PDOS in the ferromagnetic state,

the predicted change in the Fe PDOS with the Invar transition is too large, especially for phonons of short wave vectors. This may be evidence of short-range magnetic order in the LS state.

ACKNOWLEDGMENTS

We thank Brandon Keith, Jiao Lin, Chen Li, and Michael McKerns for software development and assistance. We thank Kun Woo Kim for assistance with the low-temperature NFS measurements. We thank Olivier Delaire and Max Kresch for helpful discussions. This work benefitted from the DANSE software developed under NSF Award No. DMR-0520547. This work was supported by the Department of Energy through the Carnegie-DOE Alliance Center, funded by the Department of Energy through the Stewardship Sciences Academic Alliance Program. Portions of this work were performed at HPCAT (Sector 16), Advanced Photon Source (APS), Argonne National Laboratory. HPCAT is supported by CIW, CDAC, UNLV, and LLNL through funding from DOE NNSA, DOE BES, and NSF. Use of the APS was supported by DOE BES under Contract No. DE-AC02-06CH11357.

¹K. Tanaka and K. Morioka, *Philos. Mag.* **83**, 1797 (2003).

²T. Sohmura *et al.*, *Scr. Metall.* **14**, 855 (1980); R. Oshima, *ibid.* **19**, 315 (1985).

³A. Kussmann and K. Jessen, *J. Phys. Soc. Jpn.* **17**, Suppl. B-1, 136 (1962).

⁴W. G. Stirling, R. A. Cowley, and M. W. Stringfellow, *J. Phys. F* **2**, 421 (1972).

⁵A. F. Yue, A. Papandrew, P. D. Bogdanoff, I. Halevy, J. G.-W. Lin, B. Fultz, W. Sturhahn, E. E. Alp, and T. S. Toellner, *Hyperfine Interact.* **141/142**, 249 (2002).

⁶S. Ghosh, *J. Phys. Condens. Matter* **20**, 275208 (2008).

⁷S. Baroni, S. De Gironcoli, A. Dal Corso, and P. Giannozzi, *Rev. Mod. Phys.* **73**, 515 (2001).

⁸J. M. Leger, C. Susse-Loriers, and B. Vodar, *Phys. Rev. B* **6**, 4250 (1972); G. Hausch, *Phys. Status Solidi* **16**, 371 (1973); G. Oomi and N. Mōri, *J. Phys. Soc. Jpn.* **50**, 1043 (1981); **50**, 2917 (1981); M. Sato, B. H. Grier, S. M. Shapiro, and H. Miyajima, *J. Phys. F* **12**, 2117 (1982); *J. Phys. Soc. Jpn.* **50**, 2924 (1981); M. M. Abd-Elmeguid, B. Schleede, and H. Micklitz, *J. Magn. Magn. Mater.* **72**, 253 (1988); M. M. Abd-Elmeguid and H. Micklitz, *Phys. Rev. B* **40**, 7395 (1989).

⁹L. Mañosa, G. A. Saunders, H. Rahdi, U. Kawald, J. Pelzl, and H. Bach, *Phys. Rev. B* **45**, 2224 (1992); M. Schwoerer-Böhning, S. Klotz, J. M. Besson, E. Burkel, M. Braden, and L. Pintschovius, *Europhys. Lett.* **33**, 679 (1996); S. Odin, F. Baudelet, J. P. Itié, A. Polian, S. Pizzini, A. Fontaine, Ch. Giorgetti, E. Dartyge, and J. P. Kappler, *J. Appl. Phys.* **83**, 7291 (1998); S. Odin, F. Baudelet, Ch. Giorgetti, E. Dartyge, J. P. Itié, A. Polian, J. C. Chervin, S. Pizzini, A. Fontaine, and J. P. Kappler, *Europhys. Lett.* **47**, 378 (1999).

¹⁰J. P. Rueff, A. Shukla, A. Kaprolat, M. Krisch, M. Lorenzen, F. Sette, and R. Verbeni, *Phys. Rev. B* **63**, 132409 (2001); M. Matsushita, T. Nishimura, S. Endo, M. Ishizuka, K. Kindo, and F. Ono,

J. Phys. Condens. Matter **14**, 10753 (2002); M. Matsushita, S. Endo, K. Miura, and F. Ono, *J. Magn. Magn. Mater.* **260**, 371 (2003); **269**, 393 (2004).

¹¹M. Matsushita, Y. Nakamoto, E. Suzuki, Y. Miyoshi, H. Inoue, S. Endo, T. Kikegawa, F. Ono, *J. Magn. Magn. Mater.* **284**, 403 (2004); M. Matsushita, Y. Miyoshi, S. Endo, and F. Ono, *Phys. Rev. B* **72**, 214404 (2005); F. Decremps and L. Nataf, *Phys. Rev. Lett.* **92**, 157204 (2004); L. Nataf, F. Decremps, M. Gauthier, and B. Canny, *Phys. Rev. B* **74**, 1844221 (2006).

¹²P. Gorria, D. Martinez-Blanco, M. J. Perez, J. A. Blanco, A. Hernando, M. A. Languna-Marco, D. Haskel, N. Souza-Neto, R. I. Smith, W. G. Marshall, G. Garbarino, M. Mezouar, A. Fernandez-Martinez, J. Chaboy, L. F. Barquin, J. A. Rodriguez Castrillon, M. Moldovan, J. I. G. Garcia Alonso, J. Zhang, A. Llobet, and J. S. Jiang, *Phys. Rev. B* **80**, 064421 (2009); L. Nataf, F. Decremps, J. C. Chervin, O. Mathon, S. Pascarelli, J. Kamarad, F. Baudelet, A. Congeduti, and J. P. Itie, *ibid.* **80**, 134404 (2009); B. Dutta and S. Ghosh, *Intermetallics* **18**, 1143 (2010).

¹³L. Dubrovinsky, N. Dubrovinskaia, I. A. Abrikosov, M. Vennström, F. Westman, S. Carlson, M. van Schilfgaarde, and B. Johansson, *Phys. Rev. Lett.* **86**, 4851 (2001).

¹⁴M. L. Winterrose, M. S. Lucas, A. F. Yue, I. Halevy, L. Mauger, J. A. Muñoz, J. Hu, M. Lerche, and B. Fultz, *Phys. Rev. Lett.* **102**, 237202 (2009).

¹⁵E. Sterer, M. Pasternak, and R. D. Taylor, *Rev. Sci. Instrum.* **61**, 1117 (1990).

¹⁶R. A. Forman, G. J. Piermarini, J. D. Barnett, and S. Block, *Science* **176**, 284 (1972).

¹⁷G. Longworth, *Phys. Rev.* **172**, 572 (1968).

¹⁸W. Sturhahn, T. S. Toellner, E. E. Alp, X. Zhang, M. Ando, Y. Yoda, S. Kikuta, M. Seto, and C. W. Kimball, *Phys. Rev. Lett.* **74**, 3832 (1995).

- ¹⁹H. K. Mao, J. Xu, V. V. Struzhkin, J. Shu, R. J. Hemley, W. Sturhahn, M. Y. Hu, E. E. Alp, L. Vocadlo, D. Alfè, G. D. Price, M. J. Gillan, M. Schwoerer-Böhning, D. Häusermann, P. Eng, G. Shen, H. Giefers, R. Lübbers, and G. Wortmann, *Science* **292**, 914 (2001).
- ²⁰W. Sturhahn, *Hyperfine Interact.* **125**, 149 (2000).
- ²¹M. Born and K. Huang, *Dynamical Theory of Crystal Lattices* (Clarendon, Oxford, 1954).
- ²²A. Maradudin, E. Montroll, G. Weiss, and I. Ipatova, in *Solid State Physics*, 2nd ed., edited by H. Ehrenreich, F. Seitz, and D. Turnbull (Academic, New York, 1971), Suppl. 3.
- ²³K. V. Price, R. M. Storn, and J. A. Lampinen, *Differential Evolution* (Springer, Birkhäuser, 2005).
- ²⁴M. McKerns, P. Hung, and M. Aivazis, MYSTIC: A simple model-independent inversion framework, [<http://dev.danse.us/trac/mystic>] (unpublished).
- ²⁵M. G. Kresch, California Institute of Technology, 2009.
- ²⁶G. Kresse and J. Furthmüller, *Comput. Mater. Sci.* **6**, 15 (1996); *Phys. Rev. B* **54**, 11169 (1996).
- ²⁷D. M. Ceperley and B. J. Alder, *Phys. Rev. Lett.* **45**, 566 (1980); J. P. Perdew and A. Zunger, *Phys. Rev. B* **23**, 5048 (1981).
- ²⁸P. E. Blöchl, *Phys. Rev. B* **50**, 17953 (1994); G. Kresse and D. Joubert, *ibid.* **59**, 1758 (1999).
- ²⁹F. D. Murnaghan, *Proc. Natl. Acad. Sci. USA* **30**, 244 (1944).
- ³⁰G. Kresse, J. Furthmüller, and J. Hafner, *Europhys. Lett.* **32**, 729 (1995); K. Parlinski, Z.-Q. Li, and Y. Kawazoe, *Phys. Rev. Lett.* **78**, 4063 (1997); K. Parlinski, Z. Q. Li, and Y. Kawazoe, *Phys. Rev. B* **61**, 272 (2000).
- ³¹K. Parlinski, Software PHONON,2000, [<http://wolf.ifj.edu.pl/phonon>].
- ³²J. Kaspar and D. R. Salahub, *Phys. Rev. Lett.* **47**, 54 (1981).
- ³³P. Entel, E. Hoffmann, P. Mohn, K. Schwarz, and V. L. Moruzzi, *Phys. Rev. B* **47**, 8706 (1993).